Japanese Journal of Radiology (2021) 39:186–197
https://doi.org/10.1007/s11604-020-01045-w

ORIGINAL ARTICLE

Deep learning-based and hybrid-type iterative reconstructions for CT: comparison of capability for quantitative and qualitative image quality improvements and small vessel evaluation at dynamic CE-abdominal CT with ultra-high and standard resolutions

Ryo Matsukiyo[1] · Yoshiharu Ohno[1,2] · Takahiro Matsuyama[1] · Hiroyuki Nagata[1] · Hirona Kimata[3] · Yuya Ito[3] · Yukihiro Ogawa[3] · Kazuhiro Murayama[2] · Ryoichi Kato[1] · Hiroshi Toyama[1]

Received: 19 August 2020 / Accepted: 11 September 2020 / Published online: 10 October 2020

Abstract

Purpose To determine the image quality improvement including vascular structures using deep learning reconstruction (DLR) for ultra-high-resolution CT (UHR-CT) and area-detector CT (ADCT) compared to a commercially available hybrid-iterative reconstruction (IR) method.

Materials and method Thirty-two patients suspected of renal cell carcinoma underwent dynamic contrast-enhanced (CE) CT using UHR-CT or ADCT systems. CT value and contrast-to-noise ratio (CNR) on each CT dataset were assessed with region of interest (ROI) measurements. For qualitative assessment of improvement for vascular structure visualization, each artery was assessed using a 5-point scale. To determine the utility of DLR, CT values and CNRs were compared among all UHR-CT data by means of ANOVA followed by Bonferroni post hoc test, and same values on ADCT data were also compared between hybrid IR and DLR methods by paired *t* test.

Results For all arteries except the aorta, the CT value and CNR of the DLR method were significantly higher compared to those of the hybrid-type IR method in both CT systems reconstructed as 512 or 1024 matrixes ($p < 0.05$).

Conclusion DLR has a higher potential to improve the image quality resulting in a more accurate evaluation for vascular structures than hybrid IR for both UHR-CT and ADCT.

Keywords Abdomen · Vasculature · CT · Reconstruction · Deep learning

Introduction

Minimal-invasive surgery including laparoscopic or robotic surgery is currently widely applied as one of the standard treatments for oncologic and traumatic diseases as well as acute abdominal diseases. In this procedure, accurate preoperative assessment of abdominal vascular structures including small vessels is considered as one of the essential steps for an effective and efficient abdominal surgical procedure. In the last decades, each CT vendor improved their technology continuously in the field of detector geometry with thinner slice collimation and increasing gantry rotation speed. In addition, increased temporal and spatial resolutions on a 320-detector row CT (i.e. area-detector CT: ADCT) has been reported to significantly improve visualization of small abdominal vessels and detection of anomalies as compared to a 16- or 64-detector row CT scanner [1–3].

Since 2017, ultra-high-resolution CT (UHR-CT) is available in routine clinical practice. This CT system has three different scan modes; normal resolution (NR: 0.5 mm × 80 rows/896 channels), high-resolution (HR: 0.5 mm × 80 rows/1792 channels) and super-high-resolution (SHR:

✉ Yoshiharu Ohno
yohno@fujita-hu.ac.jp

[1] Department of Radiology, Fujita Health University School of Medicine, 1-98, Dengakugakubo, Kutsukake-cho, Toyoake, Aichi 470-1192, Japan

[2] Joint Research Laboratory of Advanced Medical Imaging, Fujita Health University School of Medicine, 1-98, Dengakugakubo, Kutsukake-cho, Toyoake, Aichi 470-1192, Japan

[3] Canon Medical Systems Corporation, 1385 Shimoishigami, Otawara-shi, Tochigi 324-8550, Japan

0.25 mm × 160 rows/1792 channels), and improved spatial resolutions for UHR-CT have been reported by several investigators [4–20]. In addition, UHR-CT provides the opportunity to use larger matrix sizes such as a 1024 matrix in selected CT examinations in routine clinical practice [6, 10, 12–16, 19, 20]. However, one of the drawbacks of UHR-CT might be the relatively decreased signal-to-noise ratio (SNR) and contrast-noise ratio (CNR) due to applying a decreased detector collimation size, while using the same radiation dose protocol with standard reconstruction algorithms [21, 22].

Since 2019, deep learning reconstruction (DLR) (Advanced intelligent Clear-IQ Engine, *AiCE*, Canon Medical Systems Otawara, Japan) has become available for both UHR-CT and ADCT [23–27]. So far, no one reported the utility of DLR for image quality improvement and small vessel assessment for minimal-invasive surgery on both CT systems in the abdomen. Furthermore, the utility of DLR applied to UHR-CT images reconstructed with a 1024 matrix rather than ADCT and UHR-CT images reconstructed with a 512 matrix has not yet been addressed. Therefore, we hypothesize that DLR has a better potential than the hybrid IR for quantitative and qualitative image quality improvements and small vessel visualization on not only UHR-CT, but also ADCT in abdominal multi-detector row CT (MDCT) examinations. Moreover, UHR-CT images reconstructed with 1024 matrix show superior capability for small vessel evaluation than ADCT and UHR-CT images reconstructed with 512 matrix in patients with abdominal diseases, when applied not only hybrid IR, but also DLR methods. The purpose of this study was to determine the capability of DLR for quantitative and qualitative image quality improvement and vascular structure evaluation on abdominal contrast-enhanced MDCT examinations with UHR-CT and ADCT as compared with commercially available hybrid IR.

Materials and methods

Protocol, support, and funding

This study consisted of an in vivo and in vitro component. This retrospective study was approved by institutional review board of (Fujita Health University Hospital), and written informed consent was waved from each subject. This study was financially and technically supported by Canon Medical Systems Corporation. Three of the authors are employees of Canon Medical Systems (HK, YI, and YO), but did not have control over any of the data used in this study.

Phantom for in vitro study

For the in vitro part of the study, a commercially available phantom (Catphan-600: The Phantom Laboratory, Greenwich, NY, USA) was used. This phantom for evaluating the spatial resolution using the CTP528 model consisting of 21-line pairs per centimeter test gage, was applied to determine the utility of DLR for improving spatial resolution on UHR-CT and ADCT systems.

Subjects for in vivo study

From September 2019 to May 2020, a total of 32 patients (22 male, 10 female: mean age 61 year old) suspected of renal cell carcinoma and candidates for partial resection underwent dynamic CE-abdominal CT using UHR-CT or ADCT. Exclusion criteria were (1) contraindication of iodine contrast media administration such as allergy to iodine, toxic goiter of the thyroid and planned radioiodine treatment of thyroid cancer, (2) asthmatics, (3) cardiopulmonary complications, and (4) renal dysfunction. According to the CT systems performing dynamic CE-abdominal CT, 10 males (mean age: 65, age range 47–77 years) and 9 females (mean age: 60, age range 39–72 years) were examined as UHR-CT group, and 11 males (mean age: 58, age range 44–78 years) and 2 females (mean age: 58, age range 49–67 years) were examined as ADCT group. All patients with body weight (BW) < 70 kg were randomly assigned to either UHR-CT or ADCT by radiology technologists in our hospital, while patients with BW ≥ 70 kg were examined at ADCT system in this study. There were no significant differences in gender, age and total dose length product (DLP) between the two groups by χ^2 test. Details of patients' characteristics, the estimated volume computed tomographic dose index ($CTDI_{vol}$) at each dynamic phase and DLP for each CT examination in two groups are shown in Table 1.

CT examinations

In vitro study

A commercially available phantom with body ring was scanned 5 times by an 160-detector row UHR-CT system (Aquilion Precision, Canon Medical Systems, Otawara, Japan) and an ADCT system (Aquilion ONE Genesis Edition, Canon Medical Systems), using a 4-phase dynamic CT protocol for both systems. A UHR-CT dataset was obtained by the HR mode and applying the following parameters: 80 × 0.5 mm detector collimation, 0.813 beam pitch, 0.6 s/

Table 1 Patients' characteristics

	UHR-CT group	ADCT group	*p* value
Gender			
Male: female	10:09	11:02	0.06
Age (years)			
(Mean ± SD)	62 ± 11	58 ± 11	0.25
Hight (cm)			
(Mean ± SD)	161.4 ± 6.8	168.5 ± 9.8	0.02
Body weight (kg)			
(Mean ± SD)	58.8 ± 6.5	75.4 ± 14.9	0.0004
BMI			
(Mean ± SD)	22.6 ± 2.5	26.4 ± 3.8	0.005
BSA (m^2)			
(Mean ± SD)	1.6 ± 0.1	1.8 ± 0.2	0.001
$CTDI_{vol}$ at arterial phase (mGy)			
(Mean ± SD)	12.1 ± 0.6	22.2 ± 5.4	< 0.0001
DLP of early arterial phase (mGy cm)			
(Mean ± SD)	337.6 ± 35.2	728.4 ± 206.4	< 0.0001
Total DLP at each examination (mGy cm)			
(Mean ± SD)	2882.8 ± 582.1	3448.8 ± 934.9	0.07

BMI body mass index, *BSA* body surface area, *$CTDI_{vol}$* estimated volume computed tomographic dose index, *DLP* total dose length product

gantry rotation and 120 kVp. ADCT data were obtained with the following parameters: 80 × 0.5 mm detector collimation, 0.637 beam pitch, 0.6 s/gantry rotation and 120 kVp. Taking the averaged $CTDI_{vol}$ for in vivo imaging on both CT systems into account, tube currents, and $CTDI_{vol}$ were set as follows: UHR-CT: tube current, 240 mA, $CTDI_{vol}$, 12.4 mGy; ADCT: tube current 250 or 440 mA, $CTDI_{vol}$, 12.1 mGy or 22.4 mGy. The focus size of X-ray tube for the UHR-CT protocol was 0.4 × 0.5 mm, and for the two ADCT protocols were 0.8 × 0.9 mm for 12.4 mGy and 1.5 × 1.6 mm for 22.4 mGy. Field of view was 350 mm on both CT systems. All UHR-CT images were reconstructed with a 0.5 mm section thickness and 512 and 1024 matrix sizes, although all ADCT images were reconstructed as same section thickness and 512 matrix size. More specifically, each CT dataset was reconstructed with commercially available hybrid IR (AIDR 3D, Canon Medical Systems) as AIDR 3D Standard applying the soft tissue kernel (FC03, Canon Medical Systems) at both CT systems and DLR (*AiCE*, Canon Medical Systems) as *AiCE* Body Sharp Mild at ADCT and *AiCE* Body Mild at UHR-CT.

In vivo study

All dynamic CE-abdominal CT examinations were performed using a 4-phase dynamic CT protocol which was similar between systems. For the UHR-CT system, each phase was obtained in HR mode with the following parameters: 80 × 0.5 mm detector collimation, 0.813 beam pitch, 0.6 s/gantry rotation and 120 kVp. For the ADCT system on the other hand, each phase was obtained with the following parameters: 80 × 0.5 mm detector collimation, 0.637 beam pitch, 0.6 s/gantry rotation and 120 kVp. The focus size of X-ray tube for the UHR-CT protocol was 0.4 × 0.5 mm, and for the two ADCT protocols 0.8 × 0.9 mm. The tube current at each CT system was set by automated exposure control (AEC) (unenhanced CT: noise level, 7 Hounsfield units for section thickness of 5 mm, soft tissue kernel (FC03) and AEC reconstruction setting as AIDR 3D Standard; dual-arterial phase: noise level 4 Hounsfield units for section thickness of 5 mm, soft tissue kernel (FC03) and AEC reconstruction setting as AIDR 3D Standard; and portal or delayed phase: noise level, 8 Hounsfield units for section thickness of 5 mm, soft tissue kernel (FC03) and AEC reconstruction setting as AIDR 3D Standard). Field of view ranged from 320 to 360 mm on UHR-CT and from 320 to 360 mm on ADCT. Each subject was first examined with unenhanced CT, and this was followed by the injection of iodinated contrast medium (Iopamiron 370: Bayer Yakuhin, Co. Ltd., Osaka, Japan; Iomeprol 350: Eisai Co., Ltd., Tokyo, Japan) with a power injector (Dual Shot GX 7; Nemoto Kyorindo, Tokyo, Japan). Injection dose was 600 mg iodine per kg of body weight with afixed duration of 18 s, and followed by 25 ml of saline solution at the same rate. A bolus-tracking program was used to optimize the scanning delay for dual-arterial dynamic scans. The trigger point was placed at the abdominal aorta at the level of the celiac axis, and the trigger threshold was set at an increase in CT number of more than 200 Hounsfield units over the baseline value. The scan delays were set at 5 s after the trigger and dual-arterial dynamic images were obtained serially during a single breath hold. Portal- and delayed phase images were also obtained 90 and 240 s after injection. Then, each dynamic CE-abdominal CT data were reconstructed as 0.5 mm section thickness by the commercially available hybrid-type IR method (AIDR 3D, Canon Medical Systems) as AIDR 3D Standard by applying the soft tissue kernel (FC03, Canon Medical Systems) in both CT systems using DLR (*AiCE*, Canon Medical Systems) as *AiCE* Body Sharp Mild at ADCT and *AiCE* Body Mild at UHR-CT. In addition, All UHR-CT images were reconstructed as 512 and 1024 matrix sizes although all ADCT images were reconstructed as 512 matrix size.

Image analysis

A board-certified abdominal radiologist (RM) with 8-year experience evaluated each quantitative index in both the in vivo and in vitro scans. Another board-certified radiologist and two fellows with 6- and 7-year experiences (TM and HN) qualitatively and randomly assessed blind all dynamic

CT images without information on the type of CT scanner and reconstruction methods used. For the in vivo study, a PACS system (RapideyeCoreTFS01, Canon Medical Systems) was used for interpretation and evaluation of both quantitative and qualitative indexes.

In vitro study

To compare minimal spatial resolution between two CT systems at in vivo study, CT attenuation profiles at 1.6 mm gap phantom in the CT images of CTP528 model obtained by UHR-CT and ADCT were used to generate in precisely the same location for images reconstructed as 512 and 1024 matrix size with AIDR 3D and *AiCE*. According to previous literature [24], Image J software and its particle analysis tool (Plot Profile) were used to generate the profile curves in this study. To assess the capability for improvement of spatial resolution with UHR-CT and DLR, full width at half-maximum (FWHM), the width of the edge response of the phantom, measured by the 10–90% edge rise distance (ERD) and the edge rise slope (ERS) were measured according to Fig. 1. In addition, ERS was calculated by the following formula:

$$\mathrm{ERS} = \left(\mathrm{CT}_{90\%} - \mathrm{CT}_{10\%}\right)/\mathrm{ERD}. \quad (1)$$

$\mathrm{CT}_{90\%}$ was determined as pixel attenuation from 90% of the maximum CT attenuation and $\mathrm{CT}_{10\%}$ was evaluated as pixel attenuation from 10% of the maximum CT attenuation. The ERD and ERS were examined on both sides of the gap phantom. These measurements were performed at four different gap sites at five times (total $6 \times 5 = 30$ evaluations).

In vivo study

For quantitative assessment of image quality improvement on dynamic CE-MDCT using UHR-CT and ADCT with and without DLR, CT value and contrast-to-noise ratio (CNR) of the aorta, anterior and posterior segmental arteries of bilateral renal arteries and gastroduodenal artery were assessed using ROI measurements on all early arterial phase datasets. CNRs between each artery and psoas muscle were also determined by following formula:

$$\mathrm{CNR} = (\text{CT value at vasculature} - \text{CT value at psoas muscle})/\text{SD at psoas muscle}, \quad (2)$$

SD means standard deviation.

For qualitative assessment of improvement for vascular structure visualization at different vascular size levels, visualizations of (1) abdominal aorta, (2) celiac arterial trunk, (3) left gastric artery, (4) gastroduodenal artery, (5) dorsal pancreatic artery, (6) gastroepiploic artery, (7) inferior pyloric artery, (8) cystic artery and (9) bilateral renal arteries from segmental to interlobar arteries at early arterial phase CT images with and without DLR were assessed for both CT systems by the above-mentioned three radiologists using the following 5-point visual scoring system: 5, the artery was clearly traceable (i.e. excellent); 4, more than two-third was clearly traceable (i.e. good); 3, more than one-third was traceable (i.e. fair); 2, less than one-third was traceable (i.e. poor); and 1, the artery was untraceable (i.e. not visualized). The window level and width for each investigation were 100 Hounsfield units and 500 Hounsfield units in this study.

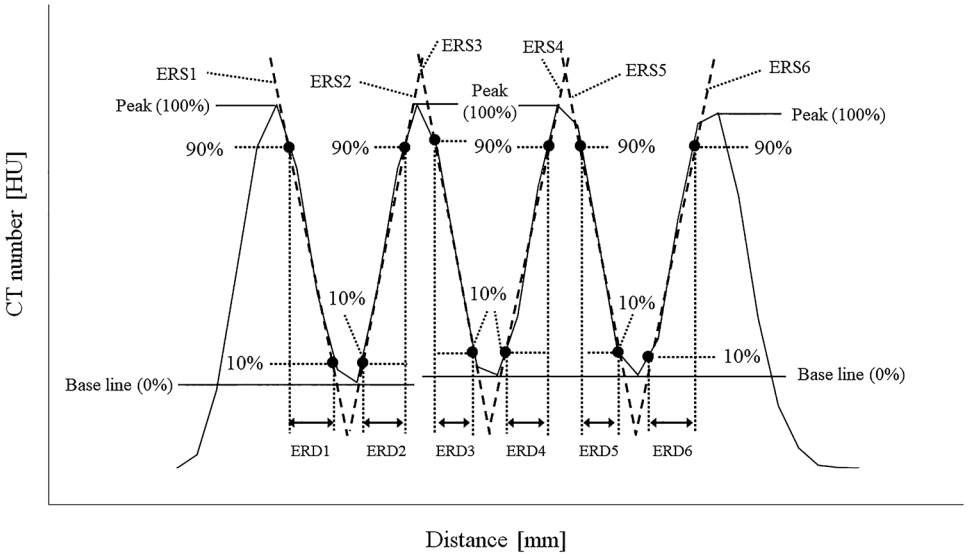

Fig. 1 Example for calculation of quantitative index evaluation for profile curve. Profile curves of the evaluated phantom. The edge rise distance (ERD) and the edge rise slope (ERS) at a pixel attenuation from 10 to 90% of the maximum CT attenuation are shown

Statistical analysis

In vitro study

To evaluate the utility of DLR method for accurate visualization of minimal spatial resolution, FWHM and ERS were compared among all UHR-CT data using analysis of variance (ANOVA) followed by Bonferroni post hoc test. Moreover, same values were also compared between ADCT reconstructed with hybrid IR and DLR by paired t test. In addition, the limits of agreement between FWHM and true value of phantom gap (i.e. 1.66 mm) of each CT data were determined by Bland–Altman analysis [28].

In vivo study

To determine the utility of DLR for quantitative image quality improvement, CT values and CNRs at aorta, all segmental renal arteries, and gastroduodenal artery were compared among all UHR-CT data by means of ANOVA followed by Bonferroni post hoc test. In addition, same values on ADCT data were also compared between hybrid-type IR and DLR methods by paired *t* test.

To evaluate the utility of DLR for image noise reduction, image noises of aorta, psoas muscle and fat on CT image were compared among all UHR-CT data by means of ANOVA followed by Bonferroni post hoc test. In addition, same values on ADCT data were also compared between hybrid-type IR and DLR methods by paired *t* test.

For assessment of the inter-observer agreements of abdominal vessel evaluations at different diameter size among three investigators, kappa statistics with χ^2 test were performed on all CT data [29]. Agreements were considered as poor for $\kappa < 0.21$, fair for $\kappa = 0.21$–0.40, moderate for $\kappa = 0.41$–0.60, substantial for $\kappa = 0.61$–0.80, and excellent for $\kappa = 0.81$–1.00 [29].

Finally, visualization score at each abdominal vessel was compared among all UHR-CT data by Steel–Dwass test. Similarly, results from ADCT were also compared between hybrid IR and DLR by Wilcoxon's signed rank test.

A p value of less than 0.05 was considered statistically significant.

Results

In vitro study

Figure 2 show all CT images of the CTP528 model on Catphan-600 for evaluating the spatial resolution and the profile curves of all CT images reconstructed with 512 or 1024 matrixes and with both reconstruction algorithms applied.

Results of compared ERS and FWHM of each CT dataset between hybrid IR and DLR and the limits of agreement between FWHM and standard deviation at each CT data are shown in Table 2. For each CT protocol, ERS was significantly smaller for DLR reconstruction than for hybrid-IR reconstructions ($p < 0.05$). In addition, ERS of UHR-CT reconstructed with a 1024 matrix was significantly higher than for 512 matrix, regardless of reconstruction algorithm ($p < 0.05$). However, the limits of agreement of each CT protocol were small enough for clinical purpose in this study.

In vivo study

Representative cases are shown in Figs. 3 and 4.

Results of the comparison of CT values and CNRs in the aorta, each segmental renal artery and gastroduodenal artery among all CT protocols are shown in Table 3. Comparison of all quantitative indexes at each segmental renal artery and gastroduodenal artery showed that the CT value and CNR of DLR reconstructions were significantly higher than of hybrid IR reconstructions for both CT systems reconstructed with either 512 or 1024 matrixes ($p < 0.05$). When comparing each index at the level of gastroduodenal artery, CT value and CNR of UHR-CT reconstructed by the same method as 1024 matrix were significantly higher than those as 512 matrix ($p < 0.05$).

Results of the image noise comparison are shown in Table 4. Image noise at the aorta, psoas muscle and fat of UHR-CT reconstructed by hybrid IR and DLR methods was significantly different in relation to matrix size ($p < 0.05$).

The assessment of inter-observer agreement for each artery between all investigators showed significantly substantial or almost perfect for all evaluations ($0.61 \leq \kappa \leq 1$, $p < 0.05$).

The scoring results for the vascular quality assessment are shown in Table 5. Comparing scores between hybrid IR and DLR, showed significant higher scores for DLR on UHR-CT reconstructions for both matrix sizes except for the aorta scoring, which scored the highest result on both types of reconstructions. On ADCT reconstructions DLR, again, scored highest for all vessels except for the gastroepiploic artery, which showed an equal scoring to the hybrid IR. UHR-CT reconstructions with hybrid IR and DLR and 1024 matrix showed significantly higher score than those as 512 matrix at all arteries except aorta ($p < 0.05$).

Discussion

Our results demonstrate that the newly developed DLR (*AiCE*) has a potential to significantly improve spatial and contrast resolution for dynamic CE-abdominal CT for UHR-CT and ADCT. In addition, we were able to demonstrate that

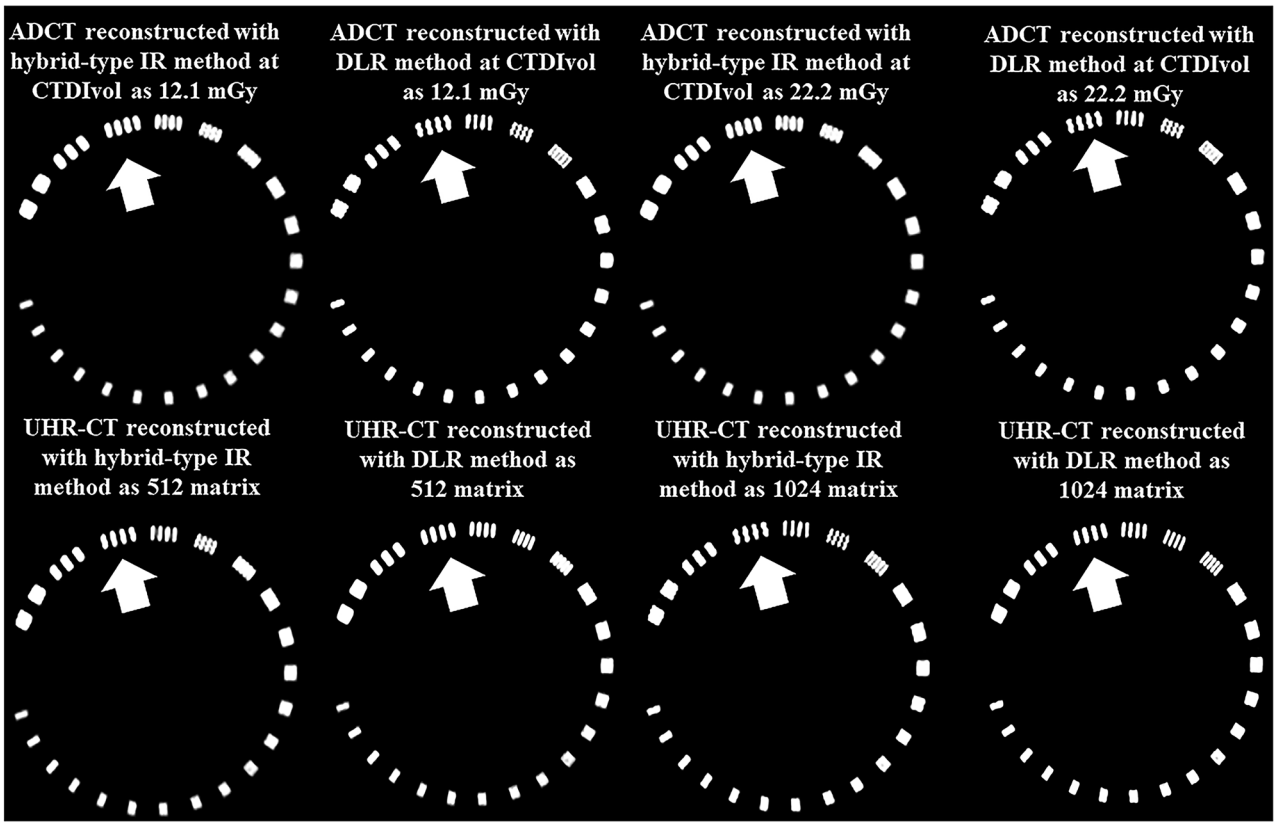

Fig. 2 CT images of the CTP528 model obtained at ultra-high-resolution CT (UHR-CT) and area-detector CT (ADCT) and reconstructed with hybrid-type IR and DLR methods and these profiles. **a** (First column, L to R: ADCT reconstructed with hybrid-type IR method at $CTDI_{vol}$ as 12.1 mGy, ADCT reconstructed with DLR at $CTDI_{vol}$ as 12.1 mGy, ADCT reconstructed with hybrid-type IR method at $CTDI_{vol}$ as 22.2 mGy and ADCT reconstructed with DLR at $CTDI_{vol}$ as 22.2 mGy; second column, L to R: UHR-CT reconstructed with hybrid-type IR method as 512 matrix, UHR-CT reconstructed with DLR as 512 matrix, UHR-CT reconstructed with hybrid-type IR method as 1024 matrix and UHR-CT reconstructed with DLR as 1024 matrix). In this study, spatial resolution phantoms (arrows) were evaluated as quantitative assessment at in vitro study. **b** (First column, L to R: profile curve on ADCT reconstructed with hybrid-type IR method at $CTDI_{vol}$ as 12.1 mGy, profile curve on ADCT reconstructed with DLR at $CTDI_{vol}$ as 12.1 mGy, profile curve on ADCT reconstructed with hybrid-type IR method at $CTDI_{vol}$ as 22.2 mGy and profile curve on ADCT reconstructed with DLR at $CTDI_{vol}$ as 22.2 mGy; second column, L to R: profile curve on UHR-CT reconstructed with hybrid-type IR method as 512 matrix, profile curve on UHR-CT reconstructed with DLR as 512 matrix, profile curve on UHR-CT reconstructed with hybrid-type IR method as 1024 matrix and profile curve on UHR-CT reconstructed with DLR as 1024 matrix). On comparison of profile curve of each CT between DLR and hybrid-type IR methods, profile curve of phantom on each CT protocol reconstructed by DLR method was more accurate than that by hybrid-type IR method

UHR-CT images reconstructed with a 1024 matrix have an improved spatial and contrast resolution compared to 512 matrix reconstructions, not only qualitatively, but also quantitatively, including smaller arteries with a size equal to or less than segmental renal arteries. To the best of our knowledge, no publication assesses the DLR and UHR-CT for both matrix sizes and image quality on vasculature in dynamic CE-abdominal CT scans of oncologic patients.

Looking at the results of spatial and contrast resolution comparisons in both in vivo and in vitro studies, DLR showed more potential than the hybrid IR for both UHR-CT and ADCT. In contrast to hybrid-type or model-based IR, which involve a trade-off between spatial resolution and noise reduction [30, 31], DLR lowers the image noise and increases spatial resolution simultaneously on a task-based model [24]. In addition, DLR was trained using a deep convolutional neural networks (DCNN) with a pair of low- and high-quality CT images. The former were obtained with low-radiation doses and subjected to hybrid IR, whereas the latter were acquired at routine doses and reconstructed with a customized model-based IR algorithm [23]. Therefore, our results were as anticipated and are fully compatible with previous studies [23–27]. Moreover, our results indicate that an improved CT value within each artery provide us with the opportunity to improve CNR of vasculature on dynamic CE-abdominal MDCT in routine clinical practice, although

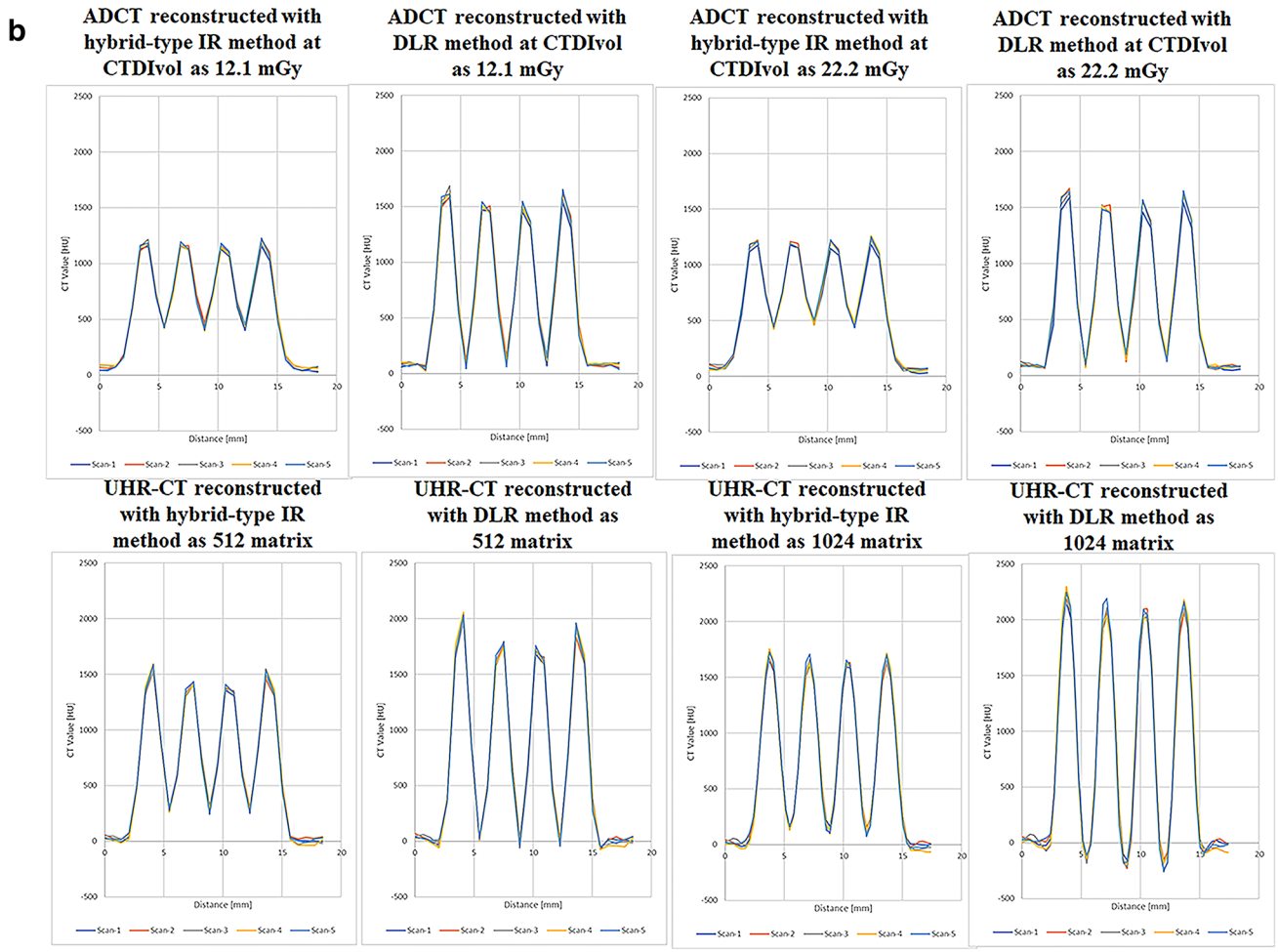

Fig. 2 (continued)

the image noise was not significant different between hybrid-type IR and DLR. Furthermore, we applied not only DLR, but also hybrid IR methods on UHR-CT and ADCT. In this study, the ADCT system uses 0.5 mm × 80 rows with 896 channels, and for the UHR-CT system, which has three different scan modes, HR mode was applied using 0.5 mm × 80 rows with 1792 channels. Therefore compared with ADCT reconstructions, improvement of spatial resolution on UHR-CT reconstructions with DLR and hybrid-type IR could be expected due to an increased channel number and basics of the CT system. Therefore, our quantitative results indicated that DLR and UHR-CT make it possible to improve visualization of abdominal vascular structures compared to conventional clinical practice.

In the qualitative assessment for abdominal vasculatures, we tested inter-observer agreements and revealed that kappa value at each vasculature between each of two readers from three investigators was significant and equal to or more than 0.61 [29]. Therefore, our qualitative assessments are considered reproducible.

Our results indicate that visual scoring at each artery on each CT protocol reconstructed by DLR was significantly higher compared to the hybrid-type IR. Moreover, UHR-CT reconstructions using hybrid-type IR and DLR with 1024 matrix showed significantly higher scores than those with 512 matrix. The quantitative results from the in vivo study are in line with the in vitro study and show comparable results to previously published results [23–27]. Therefore, the newly developed DLR (*AiCE*) are preferred in UHR-CT and ADCT for abdominal vasculature evaluation on dynamic CE-abdominal MDCT examination. In addition, preferably UHR-CT would be reconstructed as a 1024 matrix instead of a 512 matrix to improve spatial and contrast resolutions in routine clinical practice.

There are several limitations in this study. First, we used a phantom for quantitative assessment. However, this phantom is not the perfect fit for simulation of blood vessels, considering the relatively high contrast. Also nonlinear image reconstruction methods such as DLR have been reported to change their characteristics depending of

Table 2 Results of compared ERS and FWHM among all CT data and the limits of agreement between FWHM and true value of phantom gap at each CT data

Method	ERS (Mean ± SD)	FWHM (mm) (Mean ± SD)	The limits of agreement between FWHM and true value of phantom gap (mm) (Mean ± 1.96 × SD)
UHR-CT reconstructed with hybrid-type IR method as 512 matrix	864.1 ± 52.0*[a]	1.71 ± 0.02	0.04 ± 0.03
UHR-CT reconstructed with DLR method as 512 matrix	1347.2 ± 83.9[b]	1.69 ± 0.02	0.02 ± 0.05
UHR-CT reconstructed with hybrid-type IR method as 1024 matrix	1256.5 ± 52.3*	1.63 ± 0.02	− 0.04 ± 0.05
UHR-CT reconstructed with DLR method as 1024 matrix	2058.9 ± 94.3	1.60 ± 0.04	− 0.08 ± 0.08
ADCT obtained at CTDIvol as 12.1 mGy and reconstructed with hybrid-type IR method	546.5 ± 22.3*	1.74 ± 0.02	0.07 ± 0.04
ADCT obtained at CTDIvol as 12.1 mGy and reconstructed with DLR method	942.2 ± 93.0	1.73 ± 0.04	0.06 ± 0.08
ADCT obtained at CTDIvol as 22.2 mGy and reconstructed with hybrid-type IR method	548.1 ± 27.4*	1.73 ± 0.02	0.06 ± 0.04
ADCT obtained at CTDIvol as 22.2 mGy and reconstructed with DLR method	1034.6 ± 87.0	1.72 ± 0.04	0.05 ± 0.08

ERS the edge rise slope, *FWHM* full width at half-maximum, *SD* standard deviation

*Significant difference with DLR method ($p < 0.05$)

[a]Significant difference with UHR-CT reconstructed with hybrid-type IR method as 1024 matrix ($p < 0.05$)

[b]Significant difference with UHR-CT reconstructed with DLR method as 1024 matrix ($p < 0.05$)

contrast [23]. Therefore, using a phantom, which is suitable for CE-CT angiography, would be preferred in future investigation. Second, the patient number in each group was relatively small, and some physiological parameters as well as radiation dose of dynamic CE-abdominal MDCT examination differed significantly. Therefore, these facts could influence the results in our study. Third, subjects in this study, were patients who were suspected of renal cell carcinoma and candidates for partial resection. Therefore, evaluated abdominal vasculatures except the segmental renal artery were mostly in normal condition. The renal arteries, however, were affected by the invasion of renal cell carcinoma. These facts were considered as potential bias in this study. Fourth, we quantitatively and qualitatively assessed limited numbers of abdominal arteries in one phase of dynamic CE-abdominal MDCT, without evaluating portal and abdominal veins in different phases of dynamic CE-abdominal MDCT. Moreover, CTDIvols and DLPs of two CT protocols showed a significant difference, although we applied same setting of AEC at UHR-CT and ADCT systems. These facts might be caused by the upper tube current limitation for AEC modulation due to applied focus size of X-ray tube at UHR-CT system. In addition, the number of obese patient, focus size difference of the X-ray tube, kernel setting, noise reduction method, and noise reduction level setting had influence on our study results. Therefore, further investigations are warranted for determination of appropriate dynamic CT protocols as future study. Fifth, we applied a different to conventional injection protocol. The injection protocols was as follows: injection dose, 600 mg iodine per kg of body weight; since duration was fixed at 18 s with bolus-tracking delay as 5 s after the trigger; and 25 ml of saline solution at the same rate. This protocol may be considered as relative faster bolus injection protocol for dynamic CE-MDCT in abdomen and is close to thorax [32–35] and brain [13, 36], but has been determined as safe. For comparison reason across publications, it would be better to test conventional bolus injection protocol for dynamic abdominal CE-MDCT instead of current applied protocols. Therefore, further investigations are warranted for demonstration of clinical relevance of UHR-CT rather than ADCT in routine clinical practice. Sixth, while we compared DLR with hybrid-type IR we did not compare model-based IR or filtered back projection in this setting. In addition, both reconstruction methods on each CT system were compared their vasculature visualization capabilities and did not determine the detection or diagnostic capabilities of different abdominal abnormalities in each organ. Therefore, further investigation is warranted to demonstrate clinical significance of DLR for dynamic CE-abdominal MDCT examinations compared to

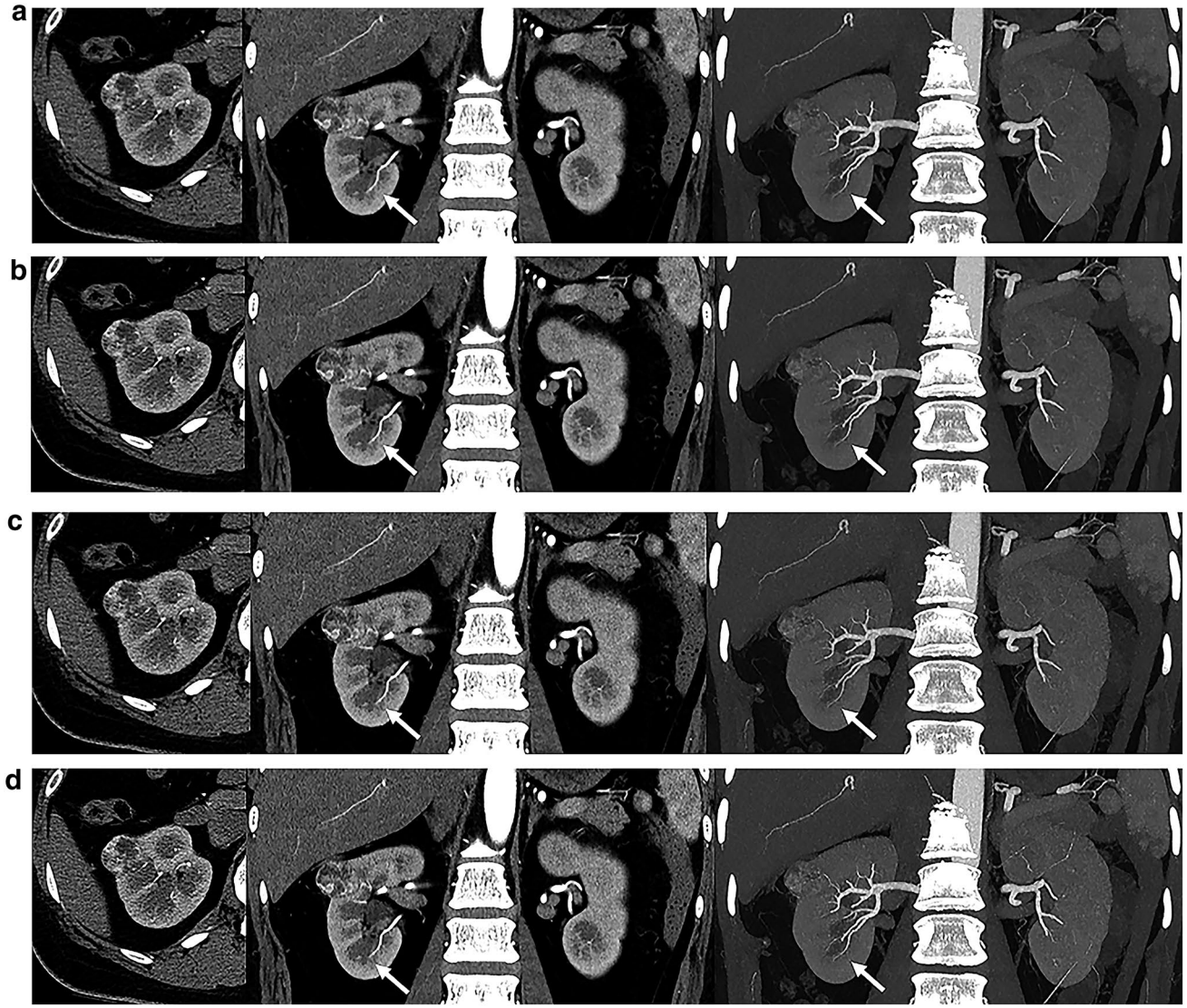

Fig. 3 UHR-CT images in 39-year old female patient with right renal cell carcinoma (L to R: axial CT image, coronal multiplanar reconstruction image and coronal maximum intensity projection image). **a** UHR-CT reconstructed with hybrid-type IR method as 512 matrix shows right inferior segmental artery and interlobar artery (arrow), and was assessed as 3. **b** UHR-CT reconstructed with DLR method as 512 matrix shows right inferior segmental artery and interlobar artery (arrow), and was assessed as 4. **c** UHR-CT reconstructed with hybrid-type IR method as 1024 matrix shows right inferior segmental artery and interlobar artery (arrow), and was assessed as 4. **d** UHR-CT reconstructed with hybrid-type IR method as 1024 matrix shows right inferior segmental artery and interlobar artery (arrow), and was assessed as 5

other reconstruction methods on UHR-CT and ADCT in both cardiovascular as oncologic patients.

In conclusion, newly developed DLR (*AiCE*) has a promising potential to quantitatively and qualitatively improve image quality and improve the evaluation on vasculature compared to hybrid-type IR (AIDR 3D) on abdominal contrast-enhanced MDCT examinations with UHR-CT reconstructed as 512 and 1024 matrices and ADCT. In addition, UHR-CT reconstructions with a 1024 matrix improve spatial and contrast resolution.

Fig. 4 ADCT images in 47-year old male patient with right renal cell carcinoma (L to R: axial CT image, coronal multiplanar reconstruction image and coronal maximum intensity projection image). **a** ADCT reconstructed with hybrid-type IR method as 512 matrix shows right superior segmental artery and interlobar artery, and was assessed as 3. **b** ADCT reconstructed with DLR method as 512 matrix shows right superior segmental artery and interlobar artery, and was assessed as 4

Table 3 Results of compared CT values and CNRs at aorta, each segmental renal artery and gastroduodenal artery

	UHR-CT reconstructed with hybrid-type IR method as 512 matrix	UHR-CT reconstructed with DLR method as 512 matrix	UHR-CT reconstructed with hybrid-type IR method as 1024 matrix	UHR-CT reconstructed with DLR method as 1024 matrix	ADCT reconstructed with hybrid-type IR method	ADCT reconstructed with DLR method
Aorta						
CT value (mean ± SD)	378.3 ± 32.5	380.0 ± 32.9	378.4 ± 32.7	379.9 ± 33.2	384.3 ± 55.8	383.7 ± 55.4
CNR (mean ± SD)	18.0 ± 2.4	17.2 ± 2.1	16.2 ± 2.2	15.2 ± 1.9	30.6 ± 7.3	27.2 ± 5.9
Each segmental renal artery						
CT value (mean ± SD)	242.9 ± 44.4*	320.6 ± 74.4	269.0 ± 48.2*	367.9 ± 91.0	219.6 ± 40.3*	278.1 ± 57.0
CNR (mean ± SD)	10.5 ± 2.5*	14.0 ± 3.7	10.7 ± 2.5*	14.6 ± 4.1	15.5 ± 4.8*	18.5 ± 5.2
Gastroduodenal artery						
CT value (mean ± SD)	177.0 ± 38.6*[a]	232.4 ± 50.4[b]	213.1 ± 43.8*	283.5 ± 63.9	102.4 ± 28.6*	143.0 ± 31.0
CNR (mean ± SD)	6.9 ± 2.2*[a]	9.4 ± 2.6[b]	8.0 ± 2.4*	10.7 ± 3.2	4.3 ± 1.9*	7.2 ± 1.8

SD standard deviation

*Significant difference with DLR method ($p < 0.05$)

[a]Significant difference with UHR-CT reconstructed with hybrid-type IR method as 1024 matrix ($p < 0.05$)

[b]Significant difference with UHR-CT reconstructed with DLR method as 1024 matrix ($p < 0.05$)

Table 4 Results of compared image noise at aorta, psoas muscle and fat

Method	UHR-CT reconstructed with hybrid-type IR method as 512 matrix	UHR-CT reconstructed with DLR method as 512 matrix	UHR-CT reconstructed with hybrid-type IR method as 1024 matrix	UHR-CT reconstructed with DLR method as 1024 matrix	ADCT reconstructed with hybrid-type IR method	ADCT reconstructed with DLR method
Aorta (mean ± SD)	20.6 ± 3.0[a]	20.3 ± 2.9[b]	22.6 ± 1.7	23.3 ± 1.6	14.0 ± 2.0	14.9 ± 1.8
Psoas muscle (mean ± SD)	18.2 ± 1.7[a]	19.2 ± 1.6[b]	20.3 ± 1.7	21.6 ± 1.6	11.1 ± 1.7	12.3 ± 1.3
Fat (mean ± SD)	16.5 ± 1.8[a]	17.0 ± 1.6[b]	18.2 ± 1.7	19.3 ± 1.7	9.8 ± 2.5	10.5 ± 1.8

SD standard deviation

*Significant difference with DLR method ($p < 0.05$)

[a]Significant difference with UHR-CT reconstructed with hybrid-type IR method as 1024 matrix ($p < 0.05$)

[b]Significant difference with UHR-CT reconstructed with DLR method as 1024 matrix ($p < 0.05$)

Table 5 Results of compared visual score at all arteries

	UHR-CT reconstructed with 512 matrix and hybrid-type IR	UHR-CT reconstructed with 512 matrix and DLR	UHR-CT reconstructed with 1024 matrix and hybrid-type IR	UHR-CT reconstructed with 1024 matrix and DLR	ADCT with hybrid-type IR method	ADCT with DLR method
Aorta (median)	5	5	5	5	4*	5
Celiac trunk (median)	4*[a]	5b	4*	5	3*	4
Renal artery (median)	3*[a]	4b	4*	5	3*	4
Lt. gastric artery (median)	3*[a]	4b	3*	5	3*	4
Gastroduodenal artery (median)	3*[a]	4b	4*	5	3*	4
Dorsal pancreatic artery (median)	3*[a]	4b	4*	4	2*	3
Gastroepiploic artery (median)	3*[a]	5b	4*	5	3*	3
Inferior pyloric artery (median)	3*[a]	4b	4*	5	2*	3
Cystic artery (median)	2*[a]	3b	3*	4	2*	3

*Significant difference with DLR method ($p < 0.05$)

[a]Significant difference with UHR-CT reconstructed with hybrid-type IR method as 1024 matrix ($p < 0.05$)

[b]Significant difference with UHR-CT reconstructed with DLR method as 1024 matrix ($p < 0.05$)

Acknowledgements Authors wish to thank Ryota Hanaoka, MD, PhD, Takashi Ichihara, PhD (Department of Radiology, Fujita Health University School of Medicine), Yujiro Doi, RT, Ryota Matsumoto RT, Akio Katagata, RT, Yumi Kataoka RT (Department of Radiology, Fujita Health University Hospital), Ryoichi Shiroki, MD, PhD (Department of Urology, Fujita Health University School of Medicine), Naruomi Akino, RT, and Kenji Fujii, RT (Canon Medical Systems Corporation) for their excellent contributions to this work. This work was financially supported by Canon Medical Systems Corporation.

Author contributions HK, YI, and YO are employees of Canon Medical Systems Corporation, who gave the suggestions for CT techniques and image analysis for in vitro study but had no control over any data or information submitted for publication nor any control over any parts of data or information included in this study.

References

1. Kitajima K, Maeda T, Ohno Y, et al. Capability of abdominal 320-detector row CT for small vasculature assessment compared with that of 64-detector row CT. Eur J Radiol. 2011;80(2):219–23.
2. Sugihara R, Kitajima K, Maeda T, et al. Comparison of capability of abdominal 320-detector row CT and of 16-detector

row CT for small vasculature assessment. Kobe J Med Sci. 2011;56(4):E154–E161161.
3. Hamamura T, Hayashida Y, Takeshita Y, et al. The usefulness of full-iterative reconstruction algorithm for the visualization of cystic artery on CT angiography. Jpn J Radiol. 2019;37(7):526–33.
4. Kakinuma R, Moriyama N, Muramatsu Y, et al. Ultra-high-resolution computed tomography of the lung: image quality of a prototype scanner. PLoS ONE. 2015;10(9):e0137165.
5. Yoshioka K, Tanaka R, Takagi H, et al. Ultra-high-resolution CT angiography of the artery of Adamkiewicz: a feasibility study. Neuroradiology. 2018;60(1):109–15.
6. Hata A, Yanagawa M, Honda O, et al. Effect of matrix size on the image quality of ultra-high-resolution CT of the lung: comparison of 512 × 512, 1024 × 1024, and 2048 × 2048. Acad Radiol. 2018;5(7):869–76.
7. Takagi H, Tanaka R, Nagata K, et al. Diagnostic performance of coronary CT angiography with ultra-high-resolution CT: comparison with invasive coronary angiography. Eur J Radiol. 2018;101:30–7.
8. Honda O, Yanagawa M, Hata A, et al. Influence of gantry rotation time and scan mode on image quality in ultra-high-resolution CT system. Eur J Radiol. 2018;103:71–5.
9. Motoyama S, Ito H, Sarai M, et al. Ultra-high-resolution computed tomography angiography for assessment of coronary artery stenosis. Circ J. 2018;82(7):1844–51.
10. Yanagawa M, Hata A, Honda O, et al. Subjective and objective comparisons of image quality between ultra-high-resolution CT and conventional area detector CT in phantoms and cadaveric human lungs. Eur Radiol. 2018;28(12):5060–8.
11. Yamashita K, Hiwatashi A, Togao O, et al. Ultrahigh-resolution CT scan of the temporal bone. Eur Arch Otorhinolaryngol. 2018;275(11):2797–803.
12. Tanabe N, Oguma T, Sato S, et al. Quantitative measurement of airway dimensions using ultra-high resolution computed tomography. Respir Investig. 2018;56(6):489–96.
13. Nagata H, Murayama K, Suzuki S, et al. Initial clinical experience of a prototype ultra-high-resolution CT for assessment of small intracranial arteries. Jpn J Radiol. 2019;37(4):283–91.
14. Tanabe N, Shima H, Sato S, et al. Direct evaluation of peripheral airways using ultra-high-resolution CT in chronic obstructive pulmonary disease. Eur J Radiol. 2019;120:108687.
15. Xu Y, Yamashiro T, Moriya H, Muramatsu S, Murayama S. Quantitative emphysema measurement on ultra-high-resolution CT scans. Int J Chron Obstruct Pulmon Dis. 2019;14:2283–90.
16. Murayama K, Suzuki S, Nagata H, Oda J, Nakahara I, Katada K, Fujii K, Toyama H. Visualization of lenticulostriate arteries on CT angiography using ultra-high-resolution CT compared with conventional-detector CT. AJNR Am J Neuroradiol. 2020;41(2):219–23.
17. Morisaka H, Shimizu Y, Adachi T, et al. Effect of ultra high-resolution computed tomography and model-based iterative reconstruction on detectability of simulated submillimeter artery. J Comput Assist Tomogr. 2020;44(1):32–6.
18. Hino T, Kamitani T, Sagiyama K, et al. Detectability of the artery of Adamkiewicz on computed tomography angiography of the aorta by using ultra-high-resolution computed tomography. Jpn J Radiol. 2020;38(7):658–65.
19. Iwasawa T, Sato M, Yamaya T, et al. Ultra-high-resolution computed tomography can demonstrate alveolar collapse in novel coronavirus (COVID-19) pneumonia. Jpn J Radiol. 2020;38(5):394–8.
20. Tsubamoto M, Hata A, Yanagawa M, et al. Ultra high-resolution computed tomography with 1024-matrix: comparison with 512-matrix for the evaluation of pulmonary nodules. Eur J Radiol. 2020;128:109033. https://doi.org/10.1016/j.ejrad.2020.109033 **(Epub 2020 Apr 29)**.
21. Kawashima H, Ichikawa K, Takata T, Nagata H, Hoshika M, Akagi N. Technical note: performance comparison of ultra-high-resolution scan modes of two clinical computed tomography systems. Med Phys. 2020;47(2):488–97.
22. Oostveen LJ, Boedeker KL, Brink M, Prokop M, de Lange F, Sechopoulos I. Physical evaluation of an ultra-high-resolution CT scanner. Eur Radiol. 2020;30(5):2552–600.
23. Higaki T, Nakamura Y, Tatsugami F, Nakaura T, Awai K. Improvement of image quality at CT and MRI using deep learning. Jpn J Radiol. 2019;37(1):73–80.
24. Tatsugami F, Higaki T, Nakamura Y, et al. Deep learning-based image restoration algorithm for coronary CT angiography. Eur Radiol. 2019;29(10):5322–9.
25. Akagi M, Nakamura Y, Higaki T, et al. Deep learning reconstruction improves image quality of abdominal ultra-high-resolution CT. Eur Radiol. 2019;29(11):6163–71.
26. Higaki T, Nakamura Y, Zhou J, et al. Deep learning reconstruction at CT: phantom study of the image characteristics. Acad Radiol. 2020;27(1):82–7.
27. Narita K, Nakamura Y, Higaki T, Akagi M, Honda Y, Awai K. Deep learning reconstruction of drip-infusion cholangiography acquired with ultra-high-resolution computed tomography. Abdom Radiol (NY). 2020. https://doi.org/10.1007/s00261-020-02508-4.
28. Bland JM, Altman DG. Statistical methods for assessing agreement between two methods of clinical measurement. Lancet. 1986;1(8476):307–10.
29. Svanholm H, Starklint H, Gundersen HJ, Fabricius J, Barlebo H, Olsen S. Reproducibility of histomorphologic diagnoses with special reference to the kappa statistic. APMIS. 1989;97(8):689–98.
30. Millon D, Vlassenbroek A, Van Maanen AG, Cambier SE, Coche EE. Low contrast detectability and spatial resolution with model-based Iterative reconstructions of MDCT images: a phantom and cadaveric study. Eur Radiol. 2017;27(3):927–37.
31. Jensen CT, Telesmanich ME, Wagner-Bartak NA, et al. Evaluation of abdominal computed tomography image quality using a new version of vendor-specific model-based iterative reconstruction. J Comput Assist Tomogr. 2017;41(1):67–74.
32. Ohno Y, Koyama H, Matsumoto K, et al. Differentiation of malignant and benign pulmonary nodules with quantitative first-pass 320-detector row perfusion CT versus FDG PET/CT. Radiology. 2011;258(2):599–609.
33. Ohno Y, Fujisawa Y, Sugihara N, et al. Dynamic contrast-enhanced perfusion area-detector CT: preliminary comparison of diagnostic performance for N stage assessment with FDG PET/CT in non-small cell lung cancer. AJR Am J Roentgenol. 2017;209(5):W253–W262262.
34. Ohno Y, Nishio M, Koyama H, et al. Solitary pulmonary nodules: comparison of dynamic first-pass contrast-enhanced perfusion area-detector CT, dynamic first-pass contrast-enhanced MR imaging, and FDG PET/CT. Radiology. 2015;274(2):563–75.
35. Ohno Y, Fujisawa Y, Yui M, et al. Solitary pulmonary nodule: comparison of quantitative capability for differentiation and management among dynamic CE-perfusion MRI at 3 T system, dynamic CE-perfusion ADCT and FDG-PET/CT. Eur J Radiol. 2019;115:22–30.
36. Murayama K, Suzuki S, Nagata H, et al. Visualization of lenticulostriate arteries on CT angiography using ultra-high-resolution CT compared with conventional-detector CT. AJNR Am J Neuroradiol. 2020;41(2):219–23.